Alexandria Engineering Journal 80 (2023) 48–57

Contents lists available at ScienceDirect

Alexandria Engineering Journal

journal homepage: www.elsevier.com/locate/aej

Original Article

A new Adomian decomposition technique for a thermal analysis forced non-Newtonian magnetic Reiner-Rivlin viscoelastic fluid flow

Amin Samimi Behbahan [a], As'ad Alizadeh [b], Meysam Mahmoudi [c], Mahmoud Shamsborhan [d], Tariq J. Al-Musawi [e], Pooya Pasha [f,*]

[a] Department of Mechanical Engineering, Behbahan Khatam Alanbia University of Technology, Behbahan, Iran
[b] Department of Civil Engineering, College of Engineering, Cihan University-Erbil, Erbil, Iraq
[c] Department of Mechanical Engineering, Engineering Faculty, Velayat University, Iranshahr, Iran
[d] Department of Mechanical Engineering, College of Engineering, University of Zakho, Zakho, Iraq
[e] Building and Construction Techniques Engineering Department, Al-Mustaqbal University College, 51001 Hillah, Babylon, Iraq
[f] Department of Mechanical Engineering, Mazandaran University of Science and Technology, Babol, Iran

ARTICLE INFO

Keywords:
Reiner-Rivlin fluid
Adomian decomposition method
Fluid flow
Magnetism amplitude

ABSTRACT

This paper presents a new semi-analytical method, called the Adomian Decomposition Method (ADM), as well as Finite Element Methods, to study forced Reiner-Rivlin non-Newtonian Magnetohydrodynamic (MHD) fluid motion confined between two disks. The innovation presented in this paper is the utilization of both analytical and numerical methods, namely ADM and FEM, to solve coupled linear differential equations, which enables the calculation and examination of parameters such as heat transfer and fluid velocity between the two disks by simplifying these equations. This model incorporates the magnetic field, and the system of partial differential equations (PDEs) acts as the governing equation in this study, which are then transformed into a set of non-linear ordinary differential equations (ODEs) using von Karman analog variables. The Adomian decomposition method can be used to solve ODEs that are related to boundary conditions. The main findings of this article suggest that as the dimensionless force parameter increases, the displacement of the fluid velocity decreases, as the particles collide with each other, the temperature gradient around the disks decreases inversely. Moreover, when the stress tensor increases, the heat transfer rate reaches its maximum value, and the transverse velocity gradient between different disks decreases.

1. Introduction

This article explores the behavior of a forced non-Newtonian MHD Reiner-Rivlin viscoelastic fluid motion model that's confined between two disks. Non-Newtonian fluids find use in diverse everyday applications. It's amazing how non-Newtonian fluids have so many practical applications in various fields like engineering, safety, and even food. The fact that the scholars were able to solve the turning disk problems by converting the partial differential equations into ODEs really showcases the power of mathematical modeling in understanding complex systems. It sounds like the scholars were able to find a solution to the two turning disk issues by converting the essential conditions into ODEs, which was necessary due to the nonlinear behavior of the partial differential conditions. This is a common challenge when working with non-Newtonian fluids, which have a variety of applications such as drag reduction, pressure technology, and even food production. Zhang et al. [1] focused on studying electro-convective instability in a viscoelastic fluid that was induced by a stable unipolar between two coaxial conduits. To make the analysis easier, Zhang et al. introduced some new factors called similarity changes that allowed them to convert partial differential equations (PDEs) into ordinary differential equations (ODEs). Karman [2], to begin with, managed the issue of the stationary viscoelastic incompressible stream on a pivoting disk. Kumar and colleagues, in their paper published in [3], examined the electromechanically driven pulsatile flow of nonlinear viscoelastic liquids, and extended their analysis to a limit. According to their findings, Kumar et al. [3] observed that the degree of flow enhancement is closely linked to the frequency and waveform of the applied actuation force. Additionally, Joens and colleagues [4] investigated the unsteady linear motion of a circle in a viscoelastic fluid. In their study, Moatimid et al. [5] investigated the nonlinear electro hydrodynamic (EHD) instability of two viscoelastic liquids under the

* Corresponding author.
E-mail address: poooyaenginer@gmail.com (P. Pasha).

https://doi.org/10.1016/j.aej.2023.08.036
Received 25 February 2023; Received in revised form 28 May 2023; Accepted 12 August 2023
Available online 24 August 2023

Nomenclature

ε	Attrition rate
τ	Shear stress
δij	Kronecker's delta
x, y	Coordinates
u, v, w	Velocity components
μnv	Coefficient of Newtonian viscosity
σ	Conductivity
η	Non-dimensional variable
k	Thermal conductivity
p	Fluid pressure (pa)
R_0	Reynolds number
M	Magnetic parameter
Ω	Rotational velocity
Cp	Specific heat
dij	physical components of the stress tensor
T	Temperature
B_0	Magnetic
T_0	Temperature of lower disk
Pr	Prandtl number
τcv	Cross-viscosity parameter

Greek symbols

ρ	Density
μ	Dynamic viscosity
Φ	Viscous-dissipation function
σ	Tension parameter
Er	Eckert Number
α	Dimensionless forced parameter
v	Kinematic viscosity

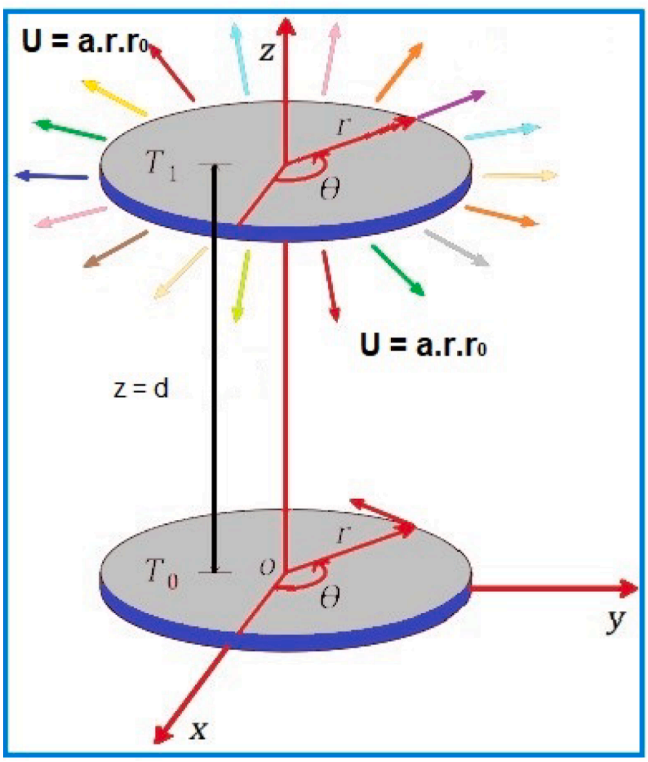

Fig. 1a. Show of two disks.

influence of mass and heat exchange. This article aims to provide a method for analyzing the nonlinear stability of a vertical cylindrical interface between two Oldroyd-B models. An unaltered pivotal electric field impacts the framework and porous medium, and the impacts of heat and mass exchange (MHT) are considered. A viscoelastic fluid is a non-Newtonian fluid consisting of a dense and elastic component. Simply put, a viscoelastic fluid is a mixture of solvent and polymer. Examples include paints, DNA suspensions, some biological fluids, and others from the chemical industry. Viscoelastic materials include amorphous polymers, semi-crystalline polymers, biopolymers, high-temperature metals, and bituminous materials. Cracking happens when a sudden strain is applied beyond the elastic limit [6–10]. Using a molecular dynamics approach, Xuefang et al. [11] studied how the atomic behavior of water-Fe3O4 nanofluids is affected by microchannel type. Burnoon et al. [12] conducted a study on natural forced cooling and utilized Monte Carlo multi-objective optimization to improve the mechanical and thermal properties of bipolar disks. These disks are intended for use in proton exchange membrane fuel cells. This study investigated the cooling, stress, and movement of bipolar disks under different environmental conditions (natural and forced cooling). A multi-objective optimization is performed under different conditions to determine the optimal thickness and number of disks to minimize temperature, stress, and displacement. Mozaffarifad and colleagues [13] conducted a numerical study on the anomalous heat conduction in the absorber disks of solar collectors. They utilized a time-resolved single-phase lag model in their investigation. Shah et al. [14] studied the effects of bio convection on the flow of Prandtl hybrid nanofluids, which includes the impact of chemical reactions and microbial movement on the tension cloth. In their study, Lou et al. [15] investigated the effect of micropolar dusty liquids on the dynamics of MHD rotating fluids when the Lorentz force is large. This course aims to analyze the effects of relevant parameters on non-Newtonian fluids and fluid dust phases. By improving the rotational parameters of the dust particle volume concentration, the axial velocity decreases in both steps. However, the temperature and transverse velocity exhibit opposite behavior in both phases. The aforementioned authors (Ashraf et al. [16]) are referred to in an academic manner. The present study investigated the utilization of biomechanics for the transportation of developing human embryos [17]. The mathematical model used the boundary layer approximation and flow assumptions to derive partial differential equations. In a scholarly study, Dey [18] analyzed the flow of viscoelastic fluid through an annular geometry, taking into account the impact of relaxation and retardation effects, as well as an external heat source/sink. To investigate viscoelastic phenomena, the Oldroyd fluid model has been used. In academic research, the process involves converting governing partial differential equations into ordinary differential equations and solving them analytically using modified Bessel functions. Reiner1 and Rivlin2 introduced a sophisticated non-Newtonian fluid that accurately predicts the outflow behavior of various materials, including biological and geological substances, polymers, and foods. A viscoelastic fluid is a non-Newtonian fluid that consists of both a viscous and an elastic component. To put it simply, it is a combination of a solvent and a polymer. Examples of substances that can be studied using this method include paints, DNA suspensions, various biological fluids, and chemicals used in industries [16,19–43]. The innovation in this article lies in the use of two analytical and numerical methods, ADM and FEM, to solve coupled linear differential equations. By simplifying the equations, these methods can calculate and examine the parameters of heat transfer and fluid velocity between the environments of two parallel disks. **The purpose of addressing this issue** in the article is to examine the

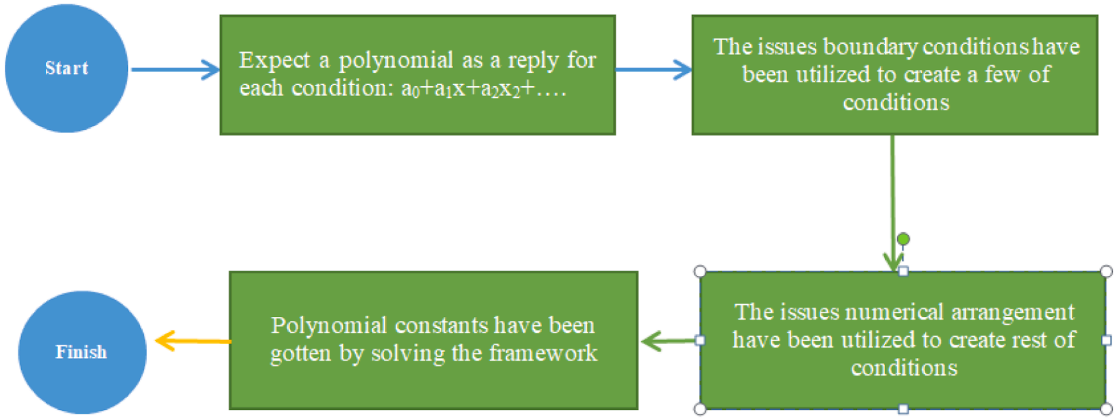

Fig. 1b. ADM techniques flow chart.

Table 1a
Comparison of f (ξ) conclusions.

ξ	ADM method	Ref [10]	FEM method
0	0	0	0
0.1	−0.062262	−0.062261	−0.06227
0.2	−0.1636412	−0.1636532	−0.1636598
0.4	−0.191444	−0.191433	−0.191467
0.6	−0.039945	−0.0.03477	−0.0.03830
0.8	0.178021	0.178089	0.178670
1	0.600000	0.6000000	0.6000000

Table 1b
Comparison of f (ξ) conclusions.

ξ	ADM method	Ref [10]	FEM method
0	0	0	0
0.1	−0.002393	−0.002491	−0.002452
0.2	−0.025454	−0.0255454	−0.025454
0.4	−0.171417	−0.171457	−0.171457
0.6	−0.055667	−0.056667	−0.055732
0.8	−0.082112	−0.082244	−0.082031
1	0	0	0

Table 1c
Comparison of h (ξ) conclusions.

ξ	ADM method	Ref [10]	FEM method
0	1	1	1
0.1	0.885088	0.886053	0.895083
0.2	0.735349	0.737141	0.735789
0.4	0.561990	0.564862	0.561901
0.6	0.350558	0.353458	0.350515
0.8	0.172401	0.173476	0.172407
1	0	0	0

behavior of non-Newtonian viscoelastic fluid flow under the influence of a magnetic field. We utilized two mathematical, analytical methods to calculate a series of critical fluid parameters, including the Reynolds number and the Prandtl number. The innovation presented in this article lies in the use of two analytical and numerical methods, ADM and FEM, to solve coupled linear differential equations. This approach simplifies the equations and enables us to calculate and examine the parameters of heat transfer and fluid velocity between the two parallel disks' environments.

Table 1d
Comparison of T* (ξ) conclusions.

ξ	ADM method	Ref [10]	FEM method
0	0	0	0
0.1	0.313002	0.313470	0.329091
0.2	0.585394	0.585324	0.592344
0.4	0.979771	0.973621	0.984661
0.6	1.396277	1.386877	1.380912
0.8	1.271326	1.271344	1.281300
1	1	1	1

1.1. Mathematical formulation

Researchers named Rainer [37] and Rivlin [38] calculated the stress tensor formula as follows:

$$\tau_{ij} = -p.\ \delta_{ij} + 2.\ \mu_{nv}.\ d_{ij} + \mu_{cv}.\ c_{ij} \tag{1}$$

Where d_{ij} and c_{ij} are:

$$d_{ij} = 1/2.\ (u_{ij} + u_{ji}),\ \ c_{ij} = d_{im}.\ d_{mj} \tag{2}$$

τij is the stretch tensor, δij is Kronecker's delta, μnv is the modulus of Newtonian viscosity and μcv is the modulus of cross viscosity, dij and cij

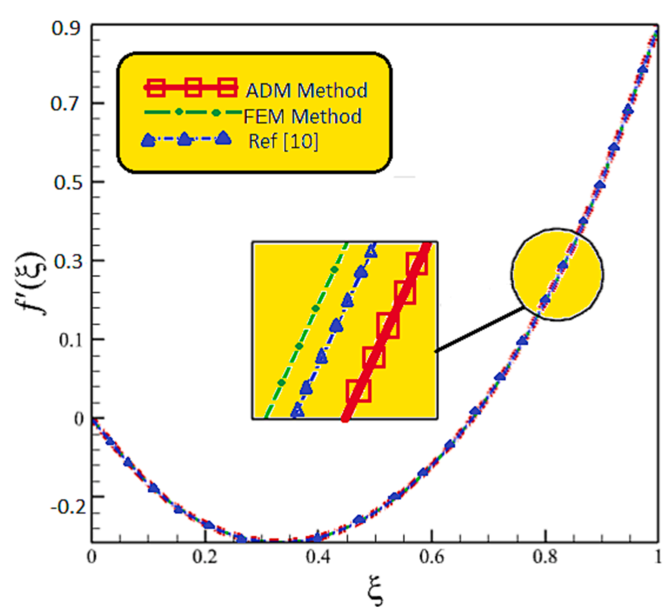

Fig. 2a. A comparison of the convergence process of the three mentioned methods.

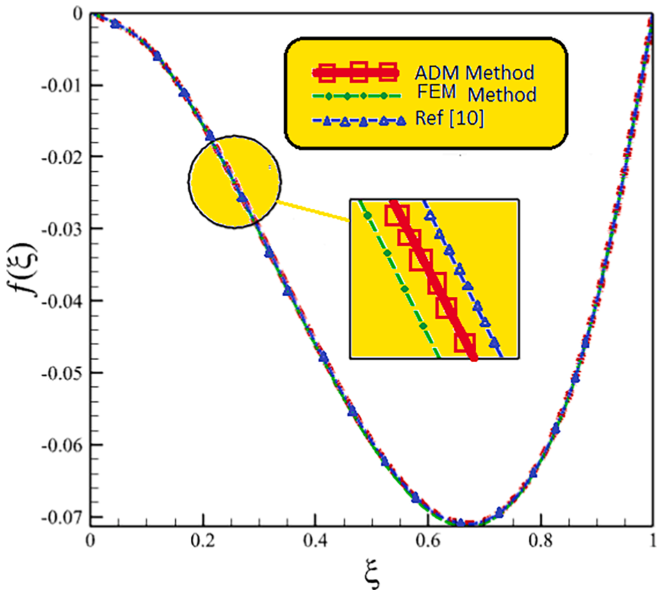

Fig. 2b. A comparison of the convergence process of the three mentioned methods for velocity.

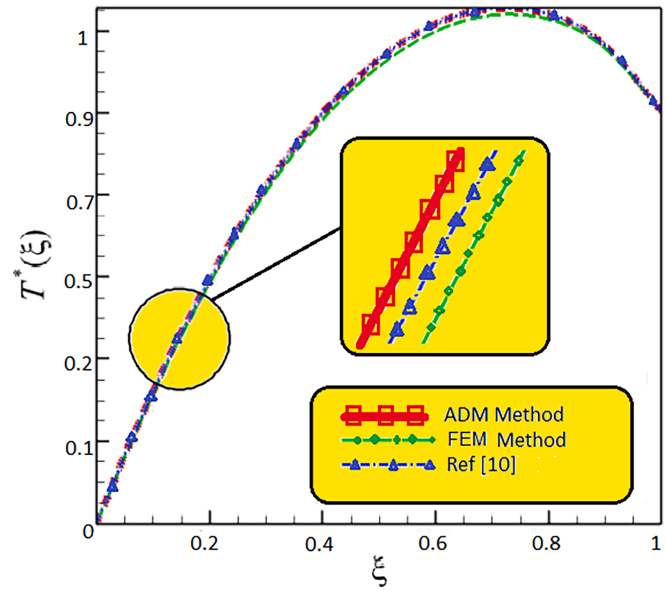

Fig. 3b. A comparison of the convergence process of the three mentioned methods for T* (ε).

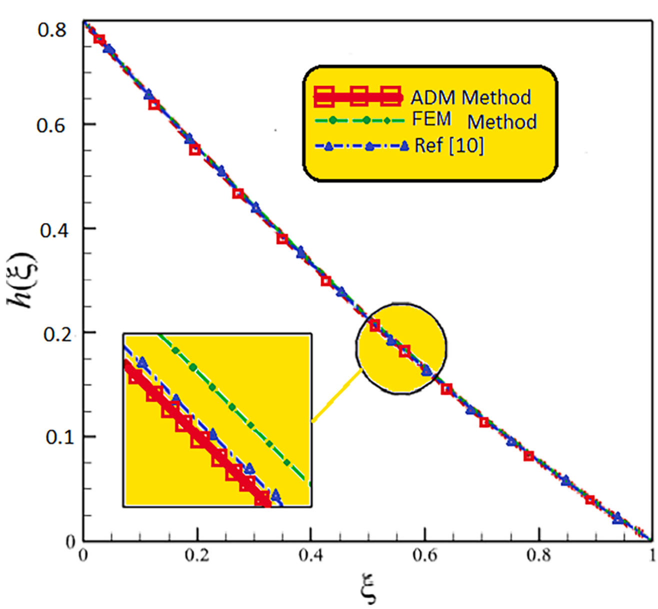

Fig. 3a. A comparison of the convergence process of the three mentioned methods for h (ε).

are the physical details of the stress tensor.

In this chapter, we investigated the conductive flow of Reiner-Rivlin fluid induced by two disks. The flow is incompressible and in a steady state. The bottom disk is located at $z = 0$, and the top disk is located at $z = d$.

A transverse magnetism square $B0$ of consistent quality is connected to the disk. The bottom disk rotates around the z axis with a constant angular velocity Ω, and the upper disk stretches with a radial velocity of ar. In this perusal, we considered a cylindrical coordinate system $\sqrt{r,\theta,z}\sqrt{}$ according to Fig. 1a. There are velocity parameters in both the (r,θ,z) and (u,v,w) directions. The bottom disk maintains a constant temperature of T_0, while the bottom is held at a steady temperature of T_1.The governing equations for momentum, continuity, and energy are:

Mass conservation in cylindrical coordinates:

$$\frac{\partial u^+}{\partial r} + \frac{u^+}{r} + \frac{\partial w^+}{\partial z} = 0 \tag{3}$$

Momentum is conserved in the r direction within a cylindrical framework:

$$\rho^+\left(u^+\frac{\partial u^+}{\partial r} - \frac{v^2}{r} + w\frac{\partial u^+}{\partial z}\right) = \frac{\partial \tau_{rr}}{\partial r} + \frac{\partial \tau_{rz}}{\partial z} + \frac{\tau_{rr} - \tau_{\theta\theta}}{r} - \frac{\sigma B_0^2 u^+}{\rho} \tag{4}$$

Conservation of momentum in the θ direction in a cylindrical coordinate system:

$$\rho^+\left(u\frac{\partial v^+}{\partial r} - \frac{u^+v^+}{r} + w\frac{\partial v^+}{\partial z}\right) = \frac{\partial \tau_{r\theta}}{\partial r} + \frac{\partial \tau_{\theta z}}{\partial z} + \frac{2\tau_{r\theta}}{r} - \frac{\sigma B_0^2 v^+}{\rho} \tag{5}$$

Conservation of momentum in the z direction in a cylindrical coordinate system:

$$\rho^+\left(u\frac{\partial w^+}{\partial r} + w^+\frac{\partial v^+}{\partial z}\right) = \frac{\partial \tau_{rz}}{\partial r} + \frac{\partial \tau_{zz}}{\partial z} + \frac{\tau_{rz}}{r} \tag{6}$$

Energy conservation in cylindrical coordinates:

$$\rho^+ c_v\left(u^+\frac{\partial T}{\partial r} + w^+\frac{\partial T}{\partial z}\right) = K\left(\frac{\partial^2 T}{\partial r^2} + \frac{1}{r}\frac{\partial T}{\partial r} + \frac{\partial^2 T}{\partial z^2}\right) + \Phi \tag{7}$$

$$\Phi = \tau_{rr}.\, d_{rr} + \tau_{\theta\theta}.\, d_{\theta\theta} + \tau_{zz}.\, d_{zz} + 2(\tau_{r\theta}.\, d_{r\theta} + \tau_{rz}.\, d_{rz} + \tau_{\theta z}.\, d_{\theta z}), \tag{8}$$

Where Φ is the viscous-dissipation function, ρ is the density, σ is the conductivity, τrr, τzz, $\tau r\theta$, $\tau z\theta$, is the components of stress tensor. k is the thermal conductivity, and T is the temperature (see Fig. 1b).

The boundary conditions for this current demonstrate are:

$$u^+ = 0,\quad = r.\,\Omega,\quad w^+ = 0,\quad T = T_0 \rightarrow z = 0\quad u^+ = ar,\quad v^+ = 0,\quad w^+ = 0,\quad T = T_1 \rightarrow z = d \tag{9}$$

Now, to convert PDEs to ODEs, we use the following analogous variables proposed by Von Karman [2].

$$u^+ = r.\,\Omega.f'(\xi),\quad v^+ = r.\,\Omega.h(\xi),\quad w^+ = -2.d\Omega.f(\xi),\quad T = (T - T_0)/T_1 - T_0, \tag{10}$$

Where $\xi = z/d$ is dimensionless variable.

The taking after temperature conveyance is proposed for Eqs. (7) and (10).

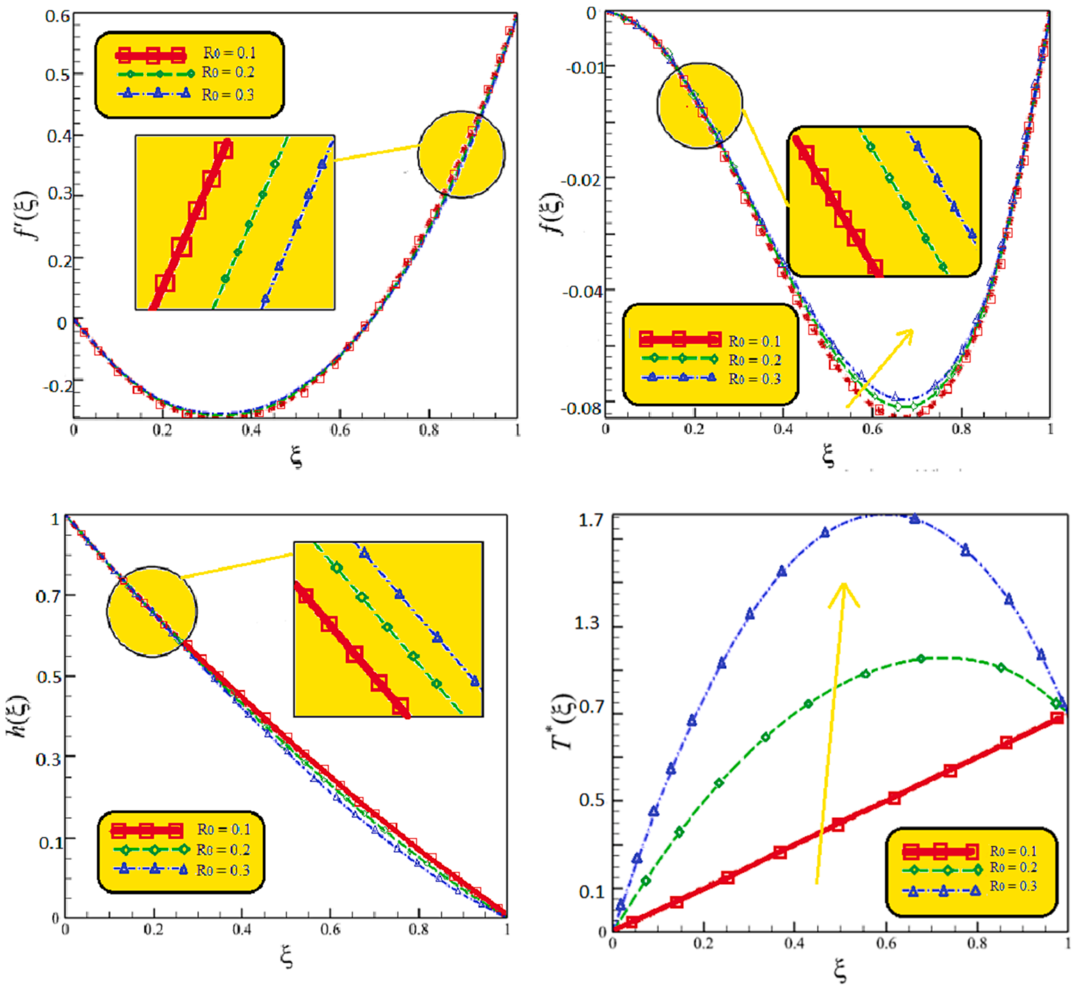

Fig. 4. The effect of Reynolds number, $R0$, on f (ξ), (ξ), $h(\xi)$ and T^* (ξ), when $\tau_{cv}=2$, $Pr=10$, $\alpha=0.6$, $M=2$, $Er=2$, $\eta=1$.

$$T=T_0+\frac{v^{+}\Omega}{c_v}\left[\phi(\xi)+\eta^2\psi(\xi)\right] \quad (11)$$

Where the $\eta=r/d$is the non-dimensional variable.

By using the similar variables in (10) for the PDEs in (4–6) and the temperature distribution in (11) for the energy equation in (7), we can derive a nonlinear ordinary differential equation:

$$f^{4}+2R_0(hh^{'}+f.hh^{'''})-2R_0\tau cv(f^{'}f(4)+3h^{'}h^{''}+f^{''}f^{'''})-M2f^{''}=0 \quad (12)$$

$$h^{''}+2R_0(f\,h^{'}+f^{'}\,h)+2R_0\tau_{cv}(f^{''}\,h^{'}+f^{'}\,h^{''})-M^2h=0 \quad (13)$$

$$\psi^{''}-P_rR_0(2f^{'}\psi-2f\psi^{'}-2f^{''}-2h^{'})-3P_rR_0\tau_{cv}(2f^{'}f^{''}+2f^{'}h^{'})=0 \quad (14)$$

$$\phi^{''}+P_rR_0(2f\,\phi^{'}+12f^{'}2)+4\psi-24P_rR_0^2\tau_{cv}f^{'}3=0 \quad (15)$$

Where $R_0=\Omega\rho d2/\mu nv$ is the Reynolds number, $P_r=\mu nvcv/k$ is the Prandtl number, $\tau cv=\mu cv/\rho d2$ is the cross-viscosity parameter and $M=(B_0^2\ \sigma d2/\mu_1)1/2$is the magnetic parameter.

Concurring to the equation, (11) the dimensionless temperature conveyance variable is:

$$T^*=\frac{T-T_0}{T_1-T_0}=E_r[\phi(\xi)+\eta^2\psi(\xi)] \quad (16)$$

Where $Er=\mu cv\Omega/(T_1-T_0)$is the Eckert number.

According to the formula. (11) The dimensionless temperature distribution variable is:

$$\begin{array}{llllll} f=0, & f^{'}=0, & h=1, & \phi=0, & \psi=0, & when\quad \xi=0 \\ f=0, & f^{'}=\alpha, & h=0, & \phi=1/E_r, & \psi=0, & when\quad \xi=01 \end{array} \quad (17)$$

Where $\alpha=a/\Omega$ is the dimensionless forced variable.

2. Simulation methodology

2.1. Dissection of the ADM technique

General nonlinear equations can be represented in the form given by [25]:

$$L(u)+Ru+Nu=g(r) \quad (18)$$

By applying the converse operator L-1 to each side of equation (49) and utilizing the given conditions [25]:

$$U=f(x)-L-1(Ru)-L-1(Nu) \quad (19)$$

In the Adomian decomposition method [25] for nonlinear differential equations, the nonlinear operator Nu = F(u) is observed.

$$F(u)=\sum_{m=0}^{\infty}A_m \quad (20)$$

The Adomian strategy characterizes the arrangement U(x) by means of a sequence [25].

$$u=\sum_{m=0}^{\infty}u_m \quad (21)$$

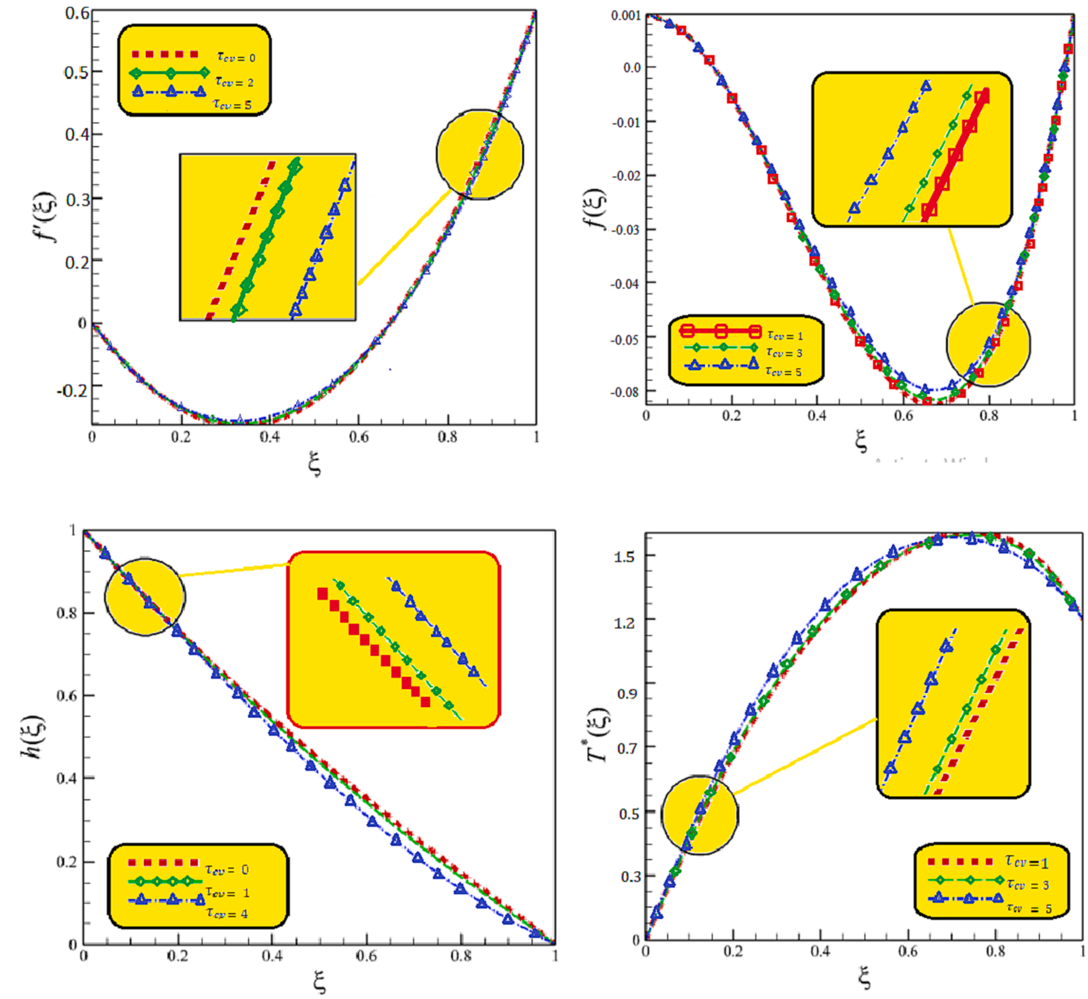

Fig. 5. The effect of the cross-viscosity parameter, τcv, on $f'(\xi)$, (ξ), $h(\xi)$ and $T^*(\xi)$, when $R_0=0.2$, $Pr=10$, $\alpha=0.6$, $M=2$, $Er=2$, $\eta=1$.

$$F(u)=F(u_0)+F'(u_0)(u-u_0)+F''(u_0)\frac{(u-u_0)}{2!}+F'''(u_0)\frac{(u-u_0)}{3!}+\cdots \tag{22}$$

After dividing the terms evenly, the first few Adomian polynomials A0, A1, A2, etc. [25] are:

$$A_0=F(u_0)$$
$$A_1=u_1F'(u_0) \qquad A_2=u_2F'(u_0)+\frac{1}{2!}u_1u_1F''(u_0) \tag{23}$$

2.2. Dissection of the FEM technique

The finite element method (FEM) is a well-known strategy for numerically solving differential equations encountered in engineering and numerical modeling. Common areas of interest include the traditional fields of structural analysis, heat transfer, fluid flow, mass transfer, and electromagnetic potential. One of the primary benefits of using the finite element method is that engineers can simulate physical phenomena, reducing the need for physical prototypes and optimizing components as part of the project's design process. The finite element method is commonly utilized in mechanical, aviation, automotive, civil engineering projects, and biomechanics.

3. Application of the ADM method

Based on the Adomian Decomposition Method, the linear portion of the equation was separated and set to 0. As a result, a differential equation with boundary conditions was solved.

$$\frac{d^4}{d\eta^4}f_0(\xi)=0 \tag{24}$$

$$\frac{d^2}{d\eta^2}h_0(\xi)=0 \tag{25}$$

$$\frac{d^2}{d\eta^2}\psi_0(\xi)=0 \tag{26}$$

$$\frac{d^2}{d\eta^2}\phi_0(\xi)=0 \tag{27}$$

$$f_0(\xi)=\xi^2-2\xi^2+\xi \leftrightarrow \psi_0(\xi)=\xi+1 \leftrightarrow \phi_0(\xi)=\xi+1 \tag{28}$$

Next, the nonlinear differential equation in Equation (12) is isolated.

$$A_0=-R_0(3\xi^2-5\xi+1)(6\xi-5) \tag{29}$$

$$B_0=R_0(\xi^2-2\xi+\xi)(6\xi-5) \tag{30}$$

$$C_0=-M(6\xi-5) \tag{31}$$

$$A_1=\left(-R_0(6\xi-5)-6R_0(3\xi^2-5\xi+1)\right)f_1(\xi) \tag{32}$$

$$B_1=\left(R_0(3\xi^2-5\xi+1)(6\xi-5)+6R_0(\xi^3-3\xi+\xi)\right)f_1(\xi) \tag{33}$$

$$C_1=-6Mf_1(\xi) \tag{34}$$

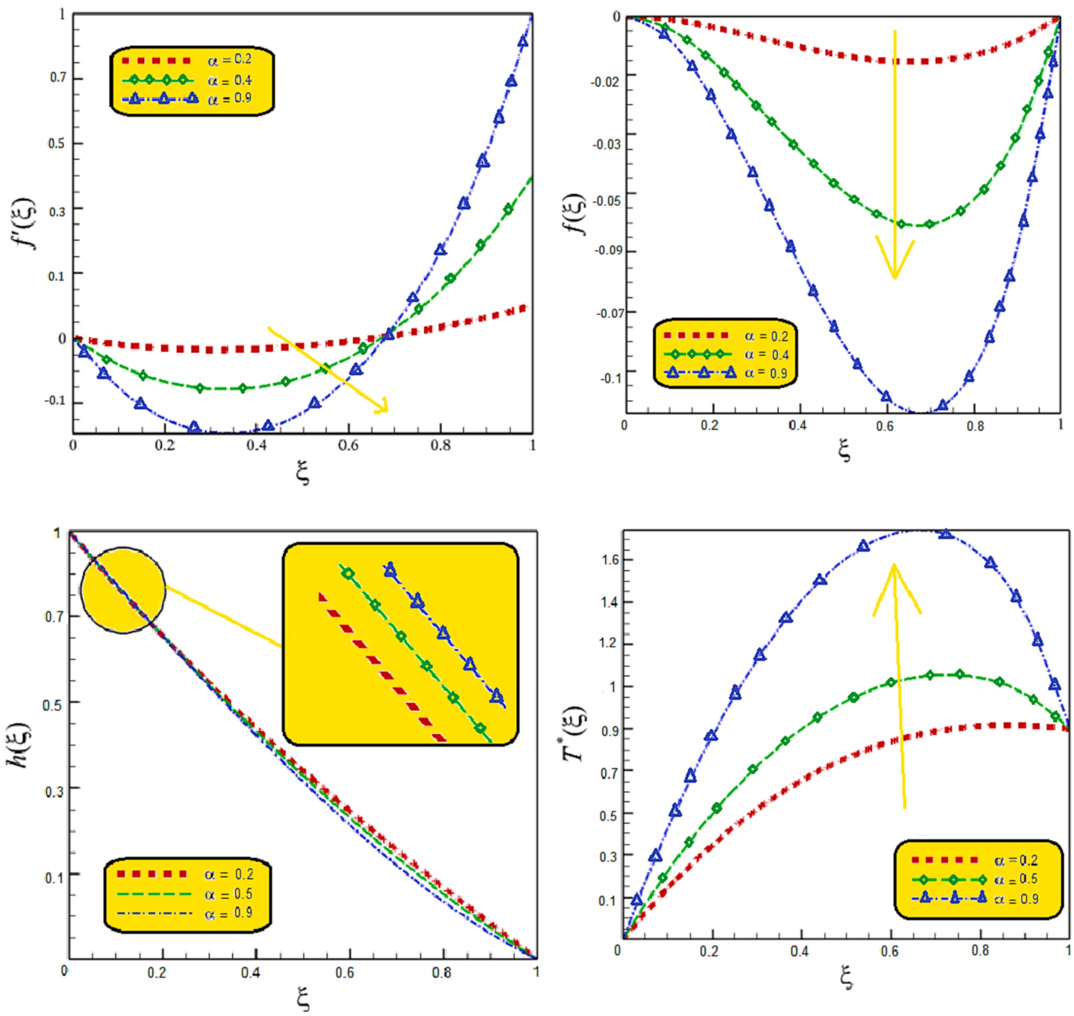

Fig. 6. The effect of the dimensionless forced parameter, α, on $f^{'}(\xi)$, (ξ), $h(\xi)$ and $T^{*}(\xi)$, when $R_0 = 0.2$, $Pr = 10$, $\tau_{cv} = 2$, $M = 2$, $Er = 2$, $\eta = 1$.

For equation (13):

$$D_0 = -\tau cvR_0(\xi^3 - 2\xi + \xi) \tag{35}$$

$$D_1 = -\tau cvR_0(3\xi^2 - 4\xi + 1)h_1(\xi) \tag{36}$$

For equation (14):

$$E_0 = -R_0pr(\xi^3 - 2\xi^2 + \xi) \tag{37}$$

$$E_1 = -R_0pr(3\xi^2 - 4\xi + 1)\psi_1(\xi) \tag{38}$$

$$E_1 = -R_0pr(3\xi^2 - 4\xi + 1)\psi_1(\xi) \tag{39}$$

According to the ADM strategy, the following values of the parameters in the equation were assumed: $\tau cv = 2$, $\alpha = 0.5$, $M = 1$, $Er = 1$, $Pr = 20$, $\eta = 1$, and $R0 = 0.1$. The ADM method solution yielded the following functions:

$$\begin{aligned} f(\xi) = {} & (0.01164396181)\xi^{12} - (0.04065039409)\xi^{11} + (0.11604434655)\xi^{10} \\ & -(0.1317874340)\xi^{9} + (0.06445920287)\xi^{8} + (0.001455306379)\xi^{7} \\ & -(0.04562227080)\xi^{6} + (0.1870027952)\xi^{5} - (0.1540473657)\xi^{4} \\ & +(0.5911555227)\xi^{3} - (0.5439795898)\xi^{2}, \end{aligned} \tag{40}$$

$$\begin{aligned} f^{'}(\xi) = {} & (0.11142795417)\xi^{11} - (0.5552943350)\xi^{10} + (1.150642655)\xi^{9} \\ & -(1.116086906)\xi^{8} + (0.6956736230)\xi^{7} + (0.05318714465)\xi^{6} \\ & -(0.3637336248)\xi^{5} + (0.6650139760)\xi^{4} - (0.6461894628)\xi^{3} \\ & +(1.763466568)\xi^{2} - (0.9379591796)\xi \end{aligned} \tag{41}$$

$$\begin{aligned} h(\xi) = {} & (0.0045209216680)\xi 10 - (0.008279781387)\xi^{9} + (0.008970858397)\xi^{8} \\ & +(0.02232372201)\xi^{7} - (0.04113552321)\xi^{6} + (0.07554752866)\xi^{5} \\ & -(0.06932690379)\xi^{4} + (0.05544621366)\xi^{3} + (0.5482399204)\xi^{2} - (1.664335601)\xi + 1, \end{aligned} \tag{42}$$

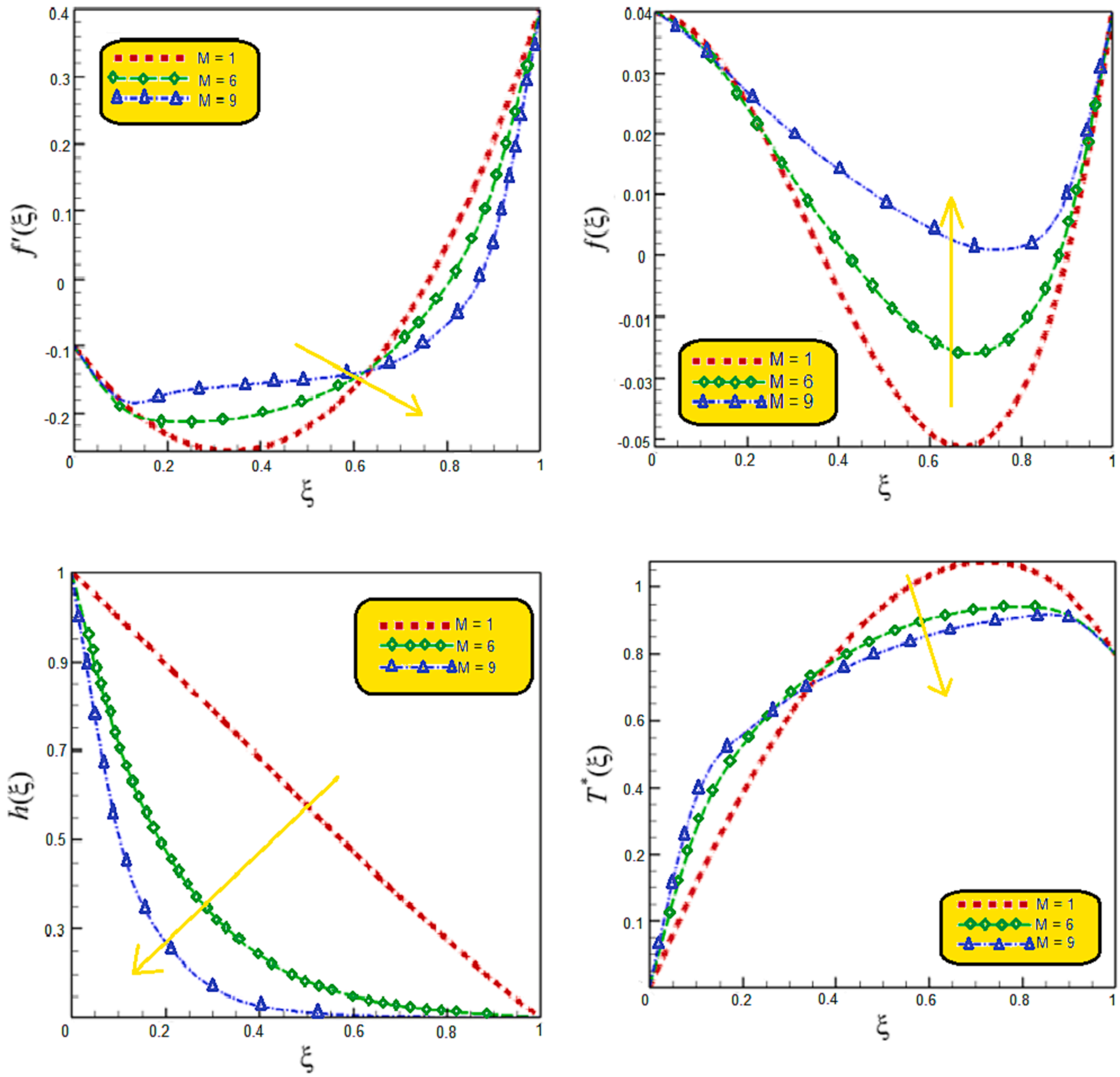

Fig. 7. The affect of the magnetic variable, on $f'(\xi)$, (ξ), $h(\xi)$ and $T^*(\xi)$, when $R0 = 0.2$, $Pr = 10$, $\tau_{cv} = 2$, $M = 2$, $Er = 2$, $\eta = 1$.

$$\begin{aligned}\psi(\xi) = {} & (0.1326813775)\xi^{10} - (0.4432527090)\xi^9 + (0.7510097656)\xi^8 \\ & -(0.8805909382)\xi^7 + (0.3653258478)\xi^6 + (0.3524606104)\xi^5 \\ & -(1.612631135)\xi^4 + (2.167942145)\xi^3 - (2.879522922)\xi^2 + (1.722344660)\xi\end{aligned} \quad (43)$$

$$\begin{aligned}\phi(\xi) = {} & (0.3260898128)\xi - (1.124418793)\xi^9 + (1.549582765)\xi^8 \\ & -(0.8479440422)\xi^7 - (1.347612264)\xi^6 + (2.724050383)\xi^5 \\ & -(0.7997274151)\xi^4 - (1.228980644)\xi^3 + (0.0018232171616)\xi^2 + (1.708138081)\xi,\end{aligned} \quad (44)$$

4. Results and discussion

In this section, we aim to confirm the accuracy of the ADM and FEM techniques by comparing them with the HPM [10], which was used for validation. We will also compare them with the respective HPM procedures. Tables and charts will be utilized to prepare the comparison. Therefore, Tables 1a–1d and Figs. 2a–3b demonstrate the accuracy of the Adomian decomposition method. Based on graphs 2 and 3, the convergence level of three modes was correctly aligned and there were no calculation errors with the least amount of error. When the values of $\tau cv = 1$, $Pr = 10$, $\alpha = 0.6$, $M = 2$, $Er = 2$, and $\eta = 1$ change, the Reynolds number R_0 will also change. As a result, the ADM arrangements of spiral velocity, pivotal velocity, transverse velocity, and temperature profile will be altered independently. The four graphs in Fig. 4 show that only the temperature profile will change significantly as the Reynolds number changes. Other parameters, such as radial, axial, and transverse, do not vary much. When the values of $R0 = 0.2$, $P = 10$, $\alpha = 0.6$, $M = 2$, Er

$= 2$, and $\eta = 1$ change, the cross-viscosity parameter τcv changes. As a result, the ADM arrangements of outspread velocity, pivotal velocity, transverse velocity, and temperature profile change individually. By conducting more frequent and continuous checks on picture number 4, we can observe that as the Reynolds number increases, the heat transfer rate reaches its maximum value, and the velocity gradient between different points also increases.

The four graphs in Fig. 5 demonstrate that there are no significant changes in radial velocity, axial velocity, transverse velocity, and temperature section when the cross-viscosity variable changes. When the dimensionless forced parameter changes (with $R0 = 0.2$, $Pr = 10$, $\tau cv = 2$, $M = 2$, $Er = 2$, $\eta = 1$ as parameters), the ADM and FEM solutions for the radial and longitudinal velocity axes, lateral velocity, and corresponding temperature profile will be affected. With more continuous checks on picture number 5, it becomes apparent that as the stress tensor increases, the heat exchange rate reaches its maximum value, and the transverse velocity gradient between different disks decreases. The four graphs in Fig. 6 illustrate that changes in the dimensionless forcing parameter lead to significant variations in the axial velocity and temperature profile, while the radial velocity remains constant. As a Magnetism parameter, M changes when $R0 = 0.2$, $Pr = 10$, $\tau cv = 2$, $\alpha = 0.6$, $Er = 2$, and $\eta = 1$. This alteration causes changes in the ADM and FEM arrangements of the spiral velocity, pivotal velocity, transverse velocity, and temperature profile, individually. Based on the results interpreted from Fig. 6, as the dimensionless force parameter increases, the displacement of fluid velocity decreases, and the collision of particles also decreases. Additionally, there is an inverse trend on the temperature gradient around the disks, leading to an increase in heat transfer between fluid particles compared to before. They are appeared in four charts compared to Fig. 7, which seems that when the Magnetic system changes, the behavior of the radial velocity, axial velocity, transverse velocity, and temperature profile will change significantly. As the effects of the magnetic boundary layer around the discs grow and continue, the fluid velocity increases accordingly, and the boundary layer becomes thicker. This increase in the growth of the velocity boundary layer and velocity gradient leads to a low heat transfer value compared to the previous states. Additionally, increasing the magnetic force results in a decrease in the transverse velocity of the fluid.

5. Conclusion

This paper presents a new semi-analytical method, called the Adomian Decomposition Method (ADM), as well as Finite Element Methods, to study forced Reiner-Rivlin non-Newtonian Magnetohydrodynamic (MHD) fluid motion confined between two disks. The innovation presented in this paper is the utilization of both analytical and numerical methods, namely ADM and FEM, to solve coupled linear differential equations, which enables the calculation and examination of parameters such as heat transfer and fluid velocity between the two disks by simplifying these equations. This model incorporates the magnetic field, and the system of partial differential equations (PDEs) acts as the governing equation in this study, which are then transformed into a set of non-linear ordinary differential equations (ODEs) using von Karman analog variables. The Adomian decomposition method can be used to solve ODEs that are related to boundary conditions. The main findings of this article suggest that as the dimensionless force parameter increases, the displacement of the fluid velocity decreases, as the particles collide with each other, the temperature gradient around the disks decreases inversely. Moreover, when the stress tensor increases, the heat transfer rate reaches its maximum value, and the transverse velocity gradient between different disks decreases.

From this paper, we can conclude that:

- This methodology demonstrates that ADM and FEM techniques can be utilized when numerical solutions for differential equations are available.
- The validation demonstrated that the ADM technique is sufficiently accurate in comparison to numerical results or previous semi-analytical methods like HPM.
- The velocities and temperature in the radial, axial, and lateral directions, as well as for different Reynolds numbers, transverse viscosity parameters, dimensionless constraint parameters, and magnetic parameter values, exhibit behavior that is similar to the published results of the HPM solution.

Declaration of Competing Interest

The authors declare that they have no known competing financial interests or personal relationships that could have appeared to influence the work reported in this paper.

Acknowledgments

The authors gratefully acknowledge the support and advice of Dr. Pooya Pasha from the Iran country, Department of mechanical Mazandaran University of science and technology. Amin Samimi Behbahan and As'ad Alizadeh: Conceived and designed the analysis. Meysam Mahmoudi: Analyzed and interpreted the data. Mahmoud Shamsborhan and Pooya Pasha: Contributed analysis tools or data. Tariq J. Al-Musawi and Pooya Pasha: Wrote the paper. Also, no funding from any institution or university has been awarded to this work.

References

[1] Z.-Y. Zhang, et al., Instability of electro convection in viscoelastic fluids induced by strong unipolar injection between two coaxial cylinders, Phys. Rev. Fluids 7 (5) (2022) 053701, https://doi.org/10.1103/PhysRevFluids.7.053701.
[2] T.V. Kármán, Über laminar und turbulent Reining, ZAMM-J. Appl. Math. Mech./ Zeitschrift für AngewandteMathematik undMechanik 1 (4) (1921) 233–252.
[3] V. Kumar, et al., Combined electromechanically driven pulsating flow of nonlinear viscoelastic fluids in narrow confinements, J. R. Soc. Interface 19 (189) (2022) 20210876, https://doi.org/10.1098/rsif.2021.0876.
[4] M.A. Joens, J.W. Swan, Unsteady and lineal translation of a sphere through a viscoelastic fluid, Phys. Rev. Fluids 7 (1) (2022) 013301, https://doi.org/10.1103/PhysRevFluids.7.013301.
[5] G.M. Moatimid, M.H. Zekry, D.A. Ibrahim, Nonlinear EHD instability of two viscoelastic fluids under the influence of mass and heat transfer, Sci. Rep. 13 (1) (2023) 357, https://doi.org/10.1038/s41598-023-27410-z.
[6] U. Hani, Comprehensive review of polymeric nanocomposite membranes application for water treatment, Alex, Eng. J. 72 (2023) 307–321, https://doi.org/10.1016/j.aej.2023.04.008.
[7] A. Zhang, Y. Wang, H. Wang, Preparation of inorganic-polymer nano-emulsion inhibitor for corrosion resistance of steel reinforcement for concrete, Alex. Eng. J. 66 (2023) 537–542, https://doi.org/10.1016/j.aej.2022.11.020.
[8] M.H. Abdel-Aziz, et al., One-dimensional ternary conducting polymers blend with 9.26% power conversion efficiency for photovoltaic devices applications, Alex. Eng. J. 66 (2023) 475–488, https://doi.org/10.1016/j.aej.2022.11.013.
[9] Z.I. Khan, et al., Mechanical and thermal properties of sepiolite strengthened thermoplastic polymer nanocomposites: a comprehensive review, Alex. Eng. J. 61 (2) (2022) 975–990, https://doi.org/10.1016/j.aej.2021.06.015.
[10] A. Larestani, et al., Predicting the surfactant-polymer flooding performance in chemical enhanced oil recovery: cascade neural network and gradient boosting decision tree, Alex. Eng. J. 61 (10) (2022) 7715–7731, https://doi.org/10.1016/j.aej.2022.01.023.
[11] X. Hu, et al., The microchannel type effects on water-Fe3O4 nanofluid atomic behavior: molecular dynamics approach, J. Taiwan Inst. Chem. Eng. 135 (2022) 104396, https://doi.org/10.1016/j.jtice.2022.104396.
[12] P. Barnoon, et al., Natural-forced cooling and Monte-Carlo multi-objective optimization of mechanical and thermal characteristics of a bipolar disk for use in a proton exchange membrane fuel cell, Energy Rep 8 (2022) 2747–2761, https://doi.org/10.1016/j.egyr.2022.01.199.
[13] M. Mozafarifard, et al., Numerical study of anomalous heat conduction in absorber disk of a solar collector using time-fractional single-phase-lag model, Case Stud. Therm. Eng. 34 (2022) 102071, https://doi.org/10.1016/j.csite.2022.102071.
[14] S.A.A. Shah, et al., Bio-convection effects on prandtl hybrid nanofluid flow with chemical reaction and motile microorganism over a stretching disk, Nanomaterials 12 (13) (2022) 2174, https://doi.org/10.3390/nano12132174.
[15] Q. Lou, et al., Micropolar dusty fluid: coriolis force effects on dynamics of MHD rotating fluid when Lorentz force is significant, Mathematics 10 (15) (2022) 2630, https://doi.org/10.3390/math10152630.
[16] H. Ashraf, et al., Flow assessment of the shear rate dependent viscoelastic fluid: application of biomechanics in growing human embryo transport, Alex. Eng. J. 60 (6) (2021) 5921–5934, https://doi.org/10.1016/j.aej.2021.04.055.

[17] S. Nadeem, et al., Numerical computations for Buongiorno nano fluid model on the boundary layer flow of viscoelastic fluid towards a nonlinear stretching sheet, Alex. Eng. J. 61 (2) (2022) 1769–1778, https://doi.org/10.1016/j.aej.2021.11.013.
[18] D. Dey, Viscoelastic fluid flow through an annulus with relaxation, retardation effects and external heat source/sink, Alex. Eng. J. 57 (2) (2018) 995–1001, https://doi.org/10.1016/j.aej.2017.01.039.
[19] M. Sheykhi, et al., Investigation of fluid viscosity and density on vibration of nano beam submerged in fluid considering nonlocal elasticity theory, Alex. Eng. J. 65 (2023) 607–614, https://doi.org/10.1016/j.aej.2022.10.016.
[20] P. Shadman, et al., Combined septum and chamfer fins on threated stretching surface under the influence of nanofluid and the magnetic parameters for rotary seals in computer hardware, Alex. Eng. J. 62 (2023) 489–507, https://doi.org/10.1016/j.aej.2022.07.044.
[21] R. Fathollahi, et al., Analyzing the effect of radiation on the unsteady 2D MHD Al2O3-water flow through parallel squeezing disks by AGM and HPM, Alex. Eng. J. (2022), https://doi.org/10.1016/j.aej.2022.11.035.
[22] N.M. Hafez, A.M. Abd-Alla, T.M.N. Metwaly, Influences of rotation and mass and heat transfer on MHD peristaltic transport of Casson fluid through inclined plane, Alex. Eng. J. 68 (2023) 665–692, https://doi.org/10.1016/j.aej.2023.01.038.
[23] P. Pasha, S. Mirzaei, M. Zarinfar, Application of numerical methods in micropolar fluid flow and heat transfer in permeable disks, Alex. Eng. J. 61 (4) (2022) 2663–2672, https://doi.org/10.1016/j.aej.2021.08.040.
[24] Z. Shoukat, et al., Impacts of joule heating with Cattaeno-Christove heat flux model in a MHD flow of Erying-Powell fluid on a Riga plate, Alex. Eng. J. 64 (2023) 741–748, https://doi.org/10.1016/j.aej.2022.10.067.
[25] S.H. Hashemi Kachapi, D.D. Ganji, Analysis of nonlinear equations in fluids, progress in nonlinear science 2 (2011).
[26] S.A. Abdollahi, et al., Investigating heat transfer and fluid flow betwixt parallel surfaces under the influence of hybrid nanofluid suction and injection with numerical analytical technique, Alex. Eng. J. 70 (2023) 423–439, https://doi.org/10.1016/j.aej.2023.02.040.
[27] B. Jalili, et al., The magnetohydrodynamic flow of viscous fluid and heat transfer examination between permeable disks by AGM and FEM, Case Stud. Therm. Eng. (2023) 102961, https://doi.org/10.1016/j.csite.2023.102961.
[28] A. Alizadeh, et al., The novelty of using the AGM and FEM for solutions of partial differential and ordinary equations along a stretchable straight cylinder, Case Stud. Therm. Eng. (2023) 102946, https://doi.org/10.1016/j.csite.2023.102946.
[29] S. Noreen, et al., Heat measures in performance of electro-osmotic flow of Williamson fluid in micro-channel, Alex. Eng. J. 59 (6) (2020) 4081–4100, https://doi.org/10.1016/j.aej.2020.07.013.
[30] Y.A. Al-Turki, et al., Numerical investigation of nanofluid flow and heat transfer in a pillow plate heat exchanger using a two-phase model: Effects of the shape of the welding points used in the pillow plate, ZAMM-J. Appl. Math. Mech./Zeitschrift für Angewandte Mathematik und Mechanik (2021), e202000300, https://doi.org/10.1002/zamm.202000300.
[31] H. Cheng, et al., The effect of temperature and external force on the thermal behavior of oil-based refrigerant inside a nanochannel using molecular dynamics simulation, J. Mol. Liq. 369 (2023) 120893, https://doi.org/10.1016/j.molliq.2022.120893.
[32] Y.-M. Li, et al., Computational hemodynamics and thermal analysis of laminar blood flow for different types of hypertension, Math. Comput. Simul 188 (2021) 330–341, https://doi.org/10.1016/j.matcom.2021.04.011.
[33] A. Alizadeh, H.J. Zekri, S. Jafarmadar, Numerical simulation of the formation of vortices around rigid cylinders as a issue of fluid-structure interaction using immersed interface method, Mechanics 26 (1) (2020) 18–24, https://doi.org/10.5755/j01.mech.26.1.23186.
[34] M. Niknejadi, et al., Numerical simulation of the thermal-hydraulic performance of solar collector equipped with vector generators filled with two-phase hybrid nanofluid Cu-TiO2/H2O, Eng. Anal. Bound. Elem. 151 (2023) 670–685, https://doi.org/10.1016/j.enganabound.2023.03.035.
[35] Y.X. Zhang, et al., Investigating the effect of size and number of layers of iron nanochannel on the thermal behavior and phase change process of calcium chloride/sodium sulfate hexa-hydrate with molecular dynamics simulation, J. Storage Mater. 62 (2023) 106762, https://doi.org/10.1016/j.est.2023.106762.
[36] H. Li, et al., A comprehensive investigation of thermal conductivity in of monolayer graphene, helical graphene with different percentages of hydrogen atom: a molecular dynamics approach, Colloids Surf. A: Physicochem. Eng. Asp. 656 (2023) 130324, https://doi.org/10.1016/j.colsurfa.2022.130324.
[37] M.R. Faridzadeh, et al., Laminar single-phase and two-phase modeling of water/MgO nanofluid flow inside a rectangular microchannel with rhombic vortex generators, ZAMM-J. Appl. Math. Mech./Zeitschrift für Angewandte Mathematik und Mechanik (2021), e202000332, https://doi.org/10.1002/zamm.202000332.
[38] J. Bai, et al., Numerical analysis and two-phase modeling of water Graphene Oxide nanofluid flow in the riser condensing tubes of the solar collector heat exchanger, Sustain. Energy Technol. Assess. 53 (2022) 102408, https://doi.org/10.1016/j.seta.2022.102408.
[39] T. Hai, D.H. Kadir, A. Ghanbari, Modeling the emission characteristics of the hydrogen-enriched natural gas engines by multi-output least-squares support vector regression: comprehensive statistical and operating analyses, Energy 276 (2023) 127515, https://doi.org/10.1016/j.energy.2023.127515.
[40] A.A. Mattie, A. Alizadeh, Using a non-conforming meshes method to simulate an interaction be-tween incompressible flow and rigid and elastic boundaries, Mechanics 25 (4) (2019) 276–282, https://doi.org/10.5755/j01.mech.25.4.22975.
[41] Y. Zhou, et al., Computational fluid dynamics and multi-objective response surface methodology optimization of perforated-finned heat sinks, J. Taiwan Inst. Chem. Eng. 145 (2023) 104823, https://doi.org/10.1016/j.jtice.2023.104823.
[42] M. Bazmi, et al., Nitrogen-doped carbon nanotubes for heat transfer applications: enhancement of conduction and convection properties of water/N-CNT nanofluid, J. Therm. Anal. Calorim. 138 (2019) 69–79, https://doi.org/10.1007/s10973-019-08024-y.
[43] A. Qasemian, et al., Hydraulic and thermal analysis of automatic transmission fluid in the presence of nano-particles and twisted tape: an experimental and numerical study, J. Cent. South Univ. 28 (11) (2021) 3404–3417, https://doi.org/10.1007/s11771-021-4864-x.